

Supplementary Information:

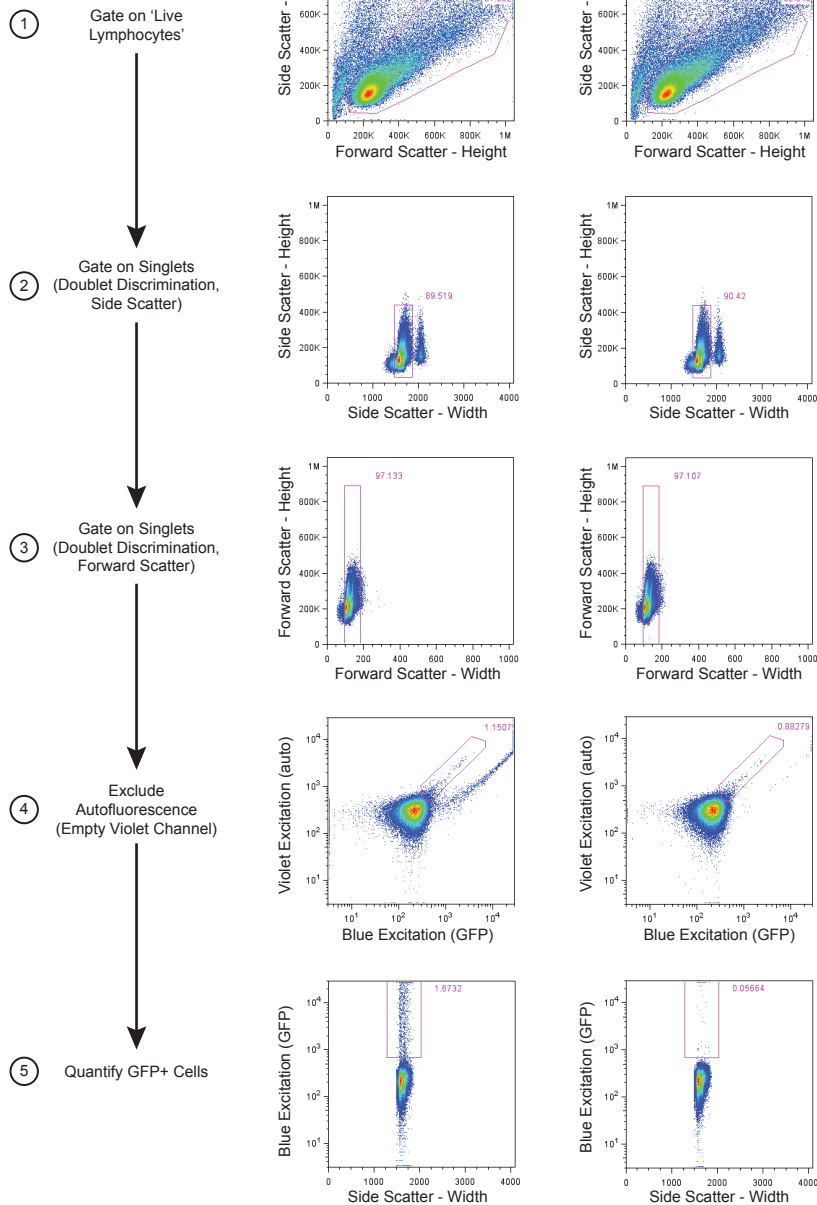
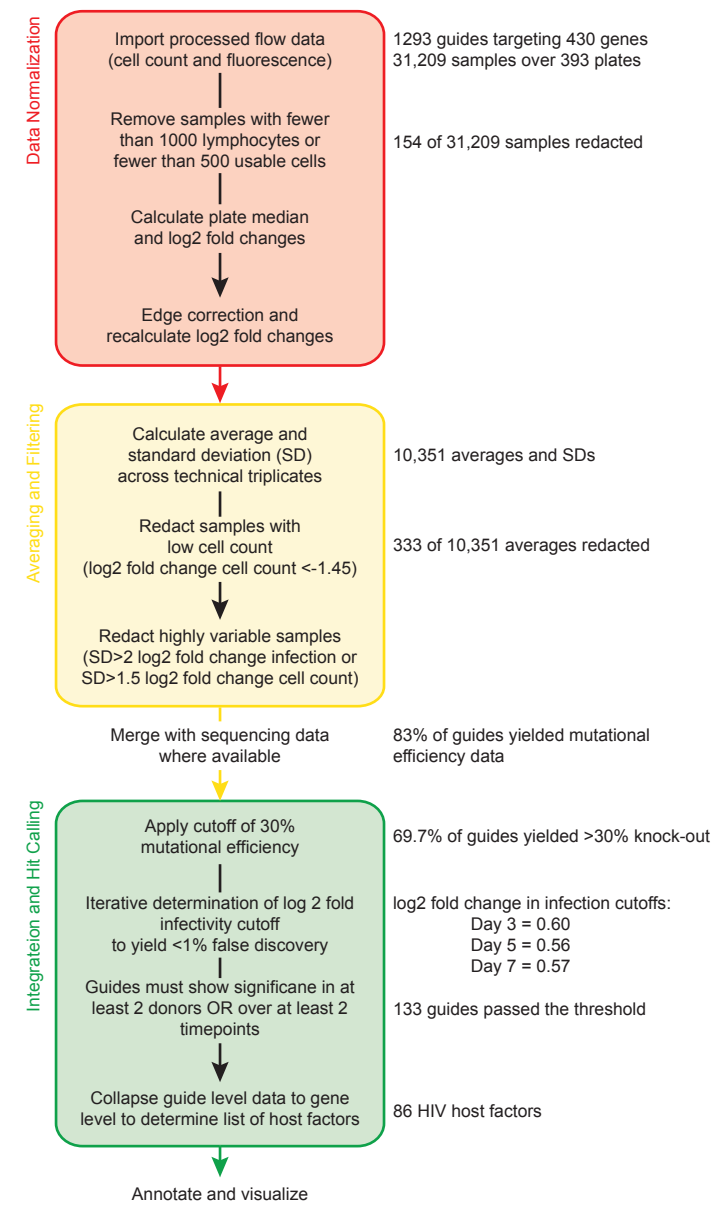
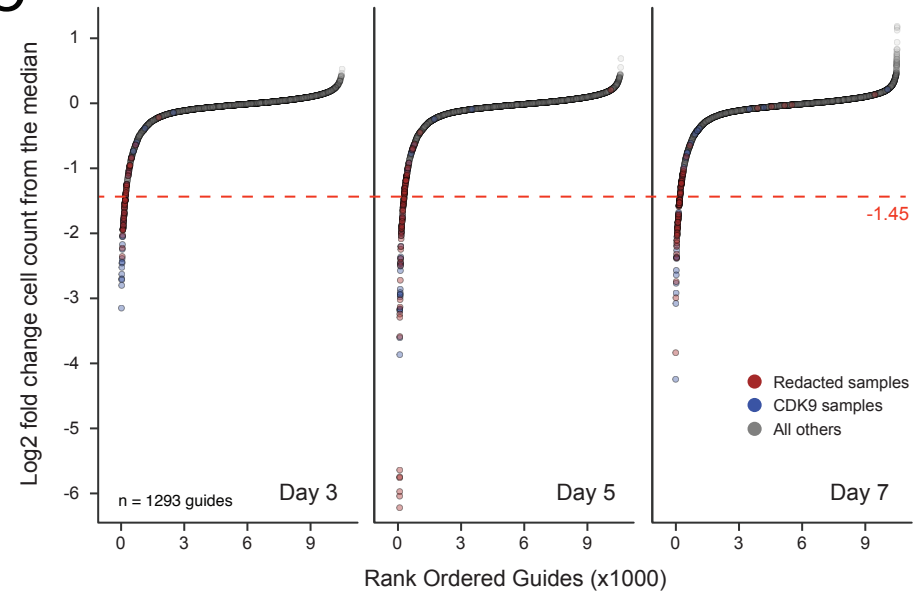
A Functional Map of HIV-Host Interactions in Primary Human T cells

Hiatt *et al.*

Supplementary Files

- 1) Supplementary Figures and Figure Legends 1-6
- 2) Supplementary References

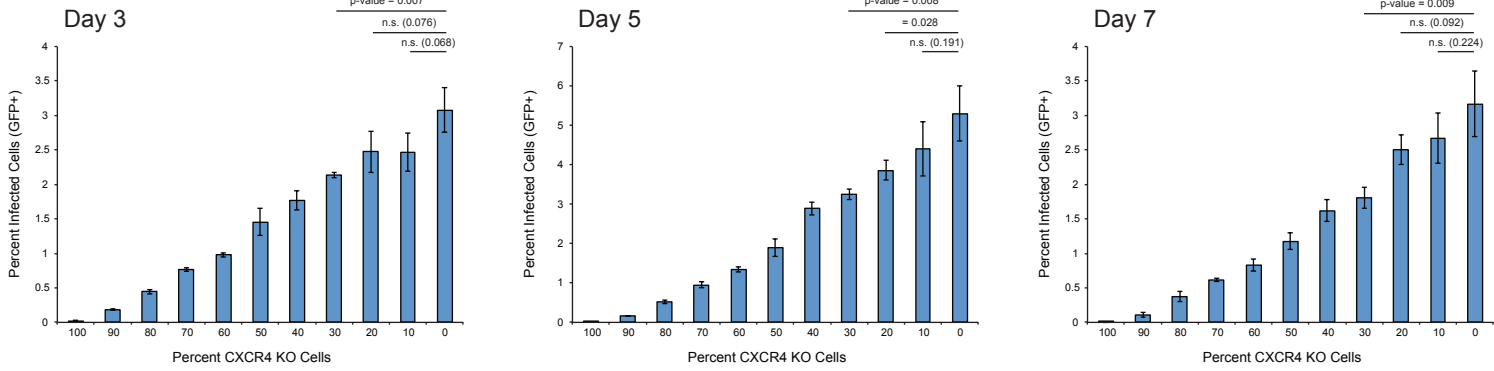
Supplementary Figure 1 | Mutational efficiency and donor-by-donor correlations. **a**, Histogram of the number of guide RNA tested in the number of unique donors, excluding control gRNA (median = 2 donors/gRNA, mean = 2.55/gRNA). **b**, Cumulative distribution function of editing efficiency for the most efficient, second most, and third most efficient guide against a given gene. Mutational efficiency was averaged across donors; guides without robust sequencing data were excluded from the plot. **c**, Heatmap of correlation of editing efficiency of guides between donors (minimum 10 guides in common, pairwise r^2 range 0.67-0.99, mean = 0.88).

A**B****C**

Supplementary Figure 2 | Data Analysis Strategy. **a**, Gating strategy for flow cytometry analysis. Representative CXCR4-targeted (right) and non-targeting control wells (left) are shown. A consistent template was used throughout analysis, with adjustment on a per-plate basis as needed. Briefly, cells were gated for lymphocytes by lightscatter followed by doublet discrimination in both side and forward scatter. Cells with equal fluorescence in the BL-1 (GFP) channel and VL-2 (AmCyan) channels were identified as auto-fluorescent and excluded from analysis. A consistent gate was then used to quantify the fraction of remaining cells that expressed GFP. **b**, Schematic of the data analysis pipeline. Briefly, individual wells were filtered for cell count and then normalized to plate median in both cell count and infection. Edge effects were corrected and plate normalization was recomputed. Technical replicates were then averaged, again filtering for low average cell count and high variability among replicates. Finally, hits were called as described. **c**, S curve plots of normalized cell count by gRNA in rank order. gRNA that were redacted from analysis due to low cell count are highlighted in red, CDK9 (a frequently redacted control) is in blue, and all others are grey. The cutoff threshold is depicted by a red dashed line.

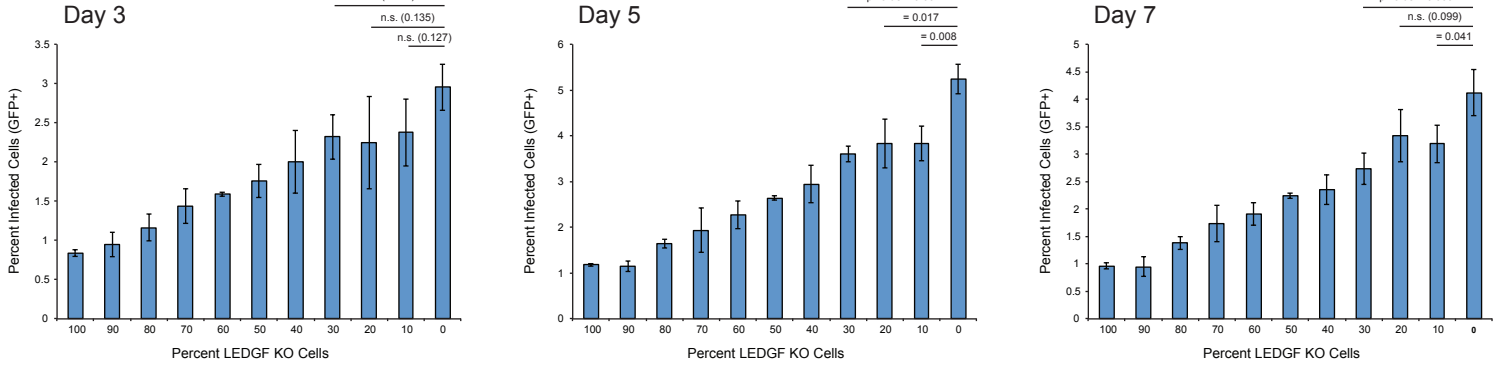
A

CXCR4



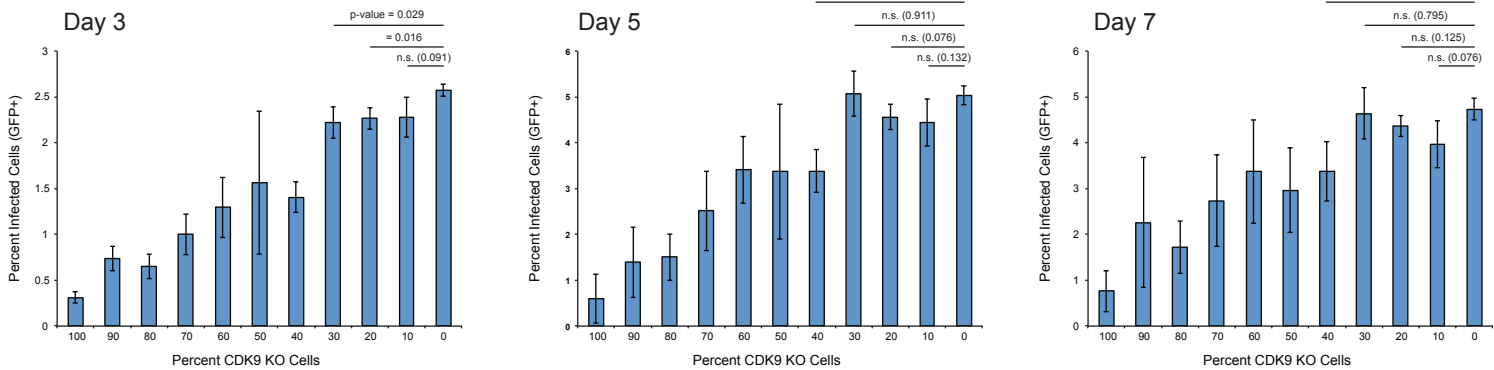
B

LEDGF

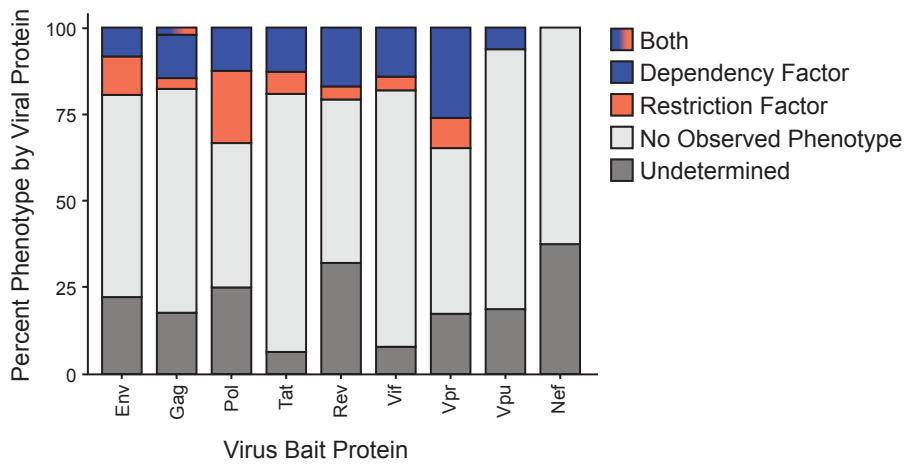
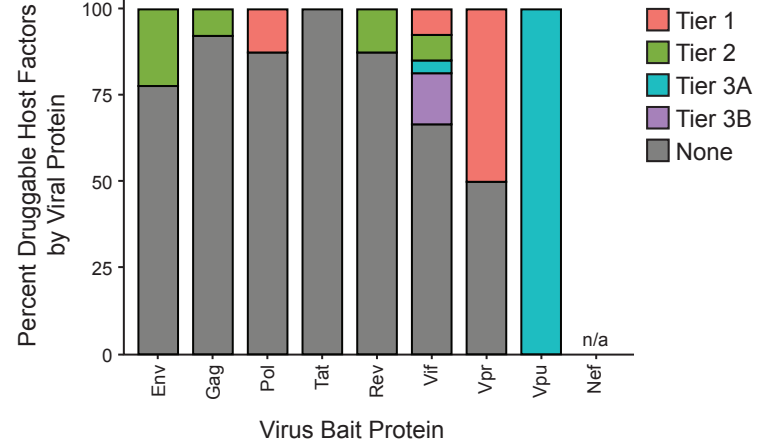
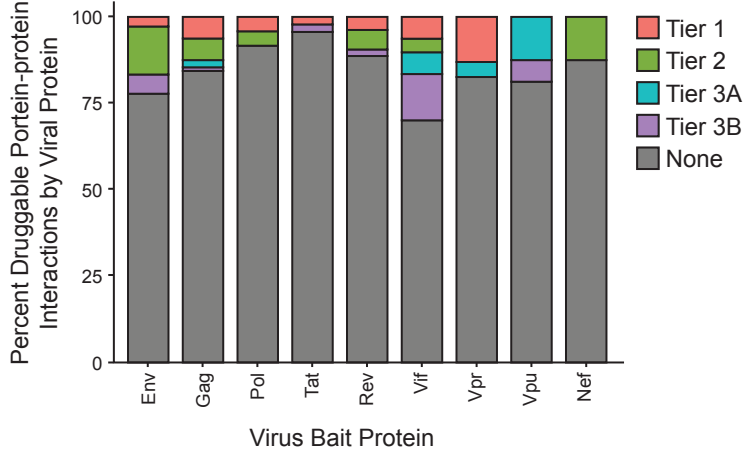
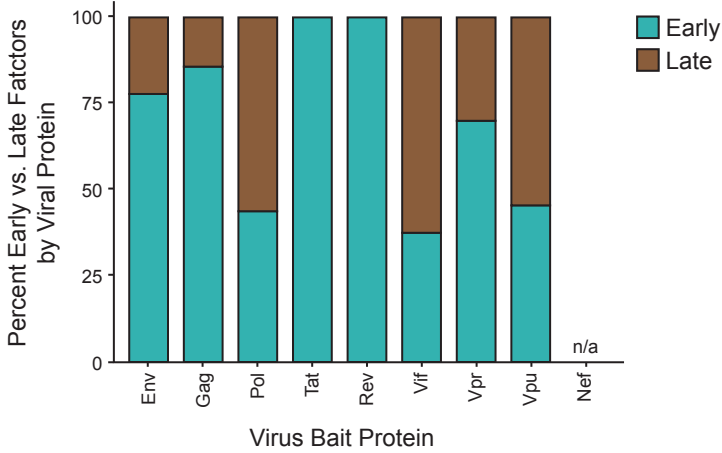


C

CDK9

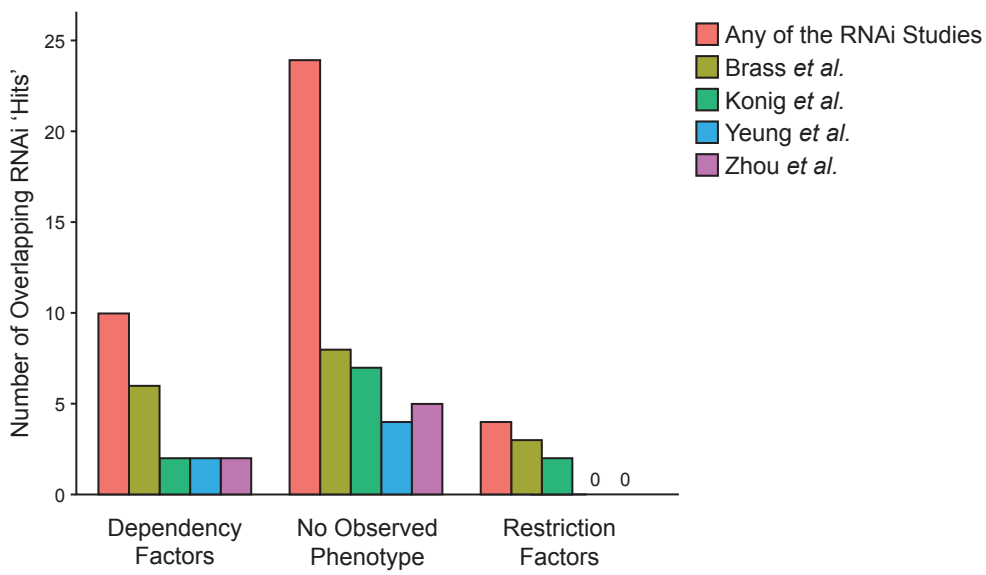


Supplementary Figure 3 | Infectivity assay sensitivity by percent edited cells and host factor. **a**, Time course of infection results for a population of non-targeting and CXCR4-knockout cells mixed at the indicated ratios (n = 3 technical triplicates, mean \pm SD). Statistical significance was determined by two-sided pairwise Student's *t*-test. The same experiment is shown for titrations of **b**, LEDGF- and **c**, CDK9-knockout cells.

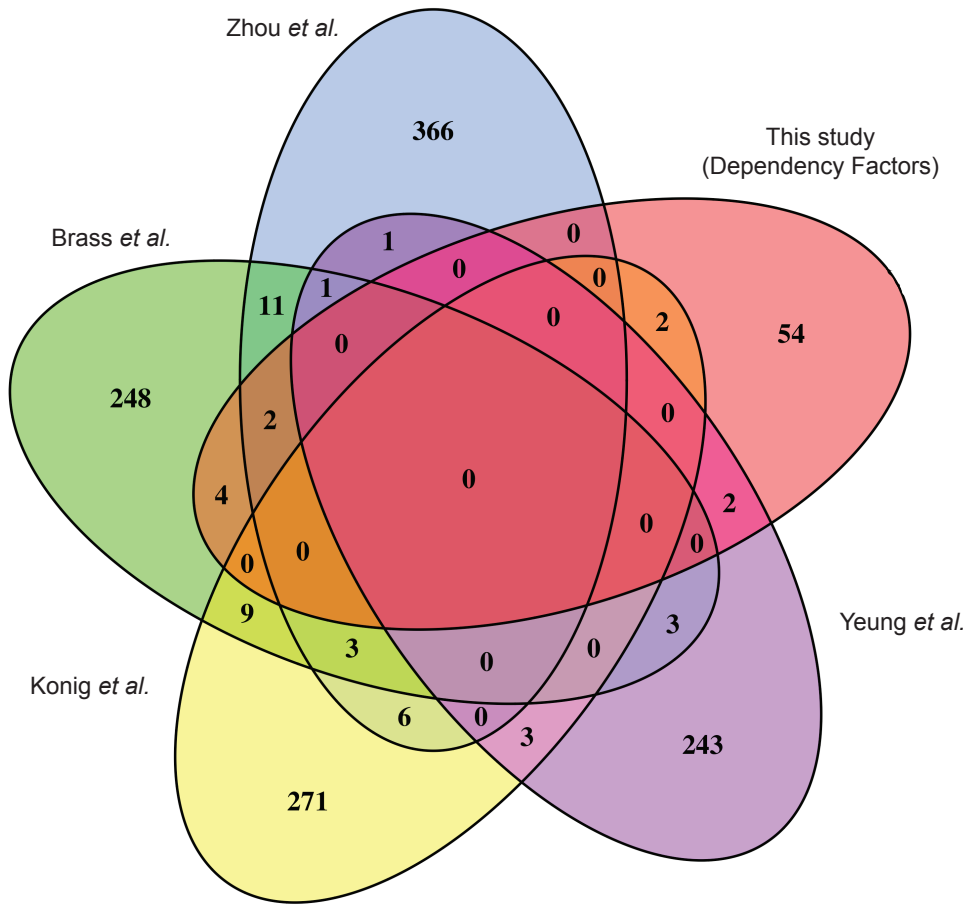
A**B****C**

Supplementary Figure 4 | Classification of targeted genes by HIV polyprotein interactor and phenotype. **a**, Experimentally-determined phenotype of targeted host genes in the screen, sorted by HIV bait. **b**, Druggability of all targeted genes, according to published classification (left) and druggability of hits from the screen, according to published classification (right)¹. **d**, Stacked cumulative bar graph of hits classified by having an early (significant on day 3) versus late (significant on days 5 or 7) phenotype by HIV bait.

A

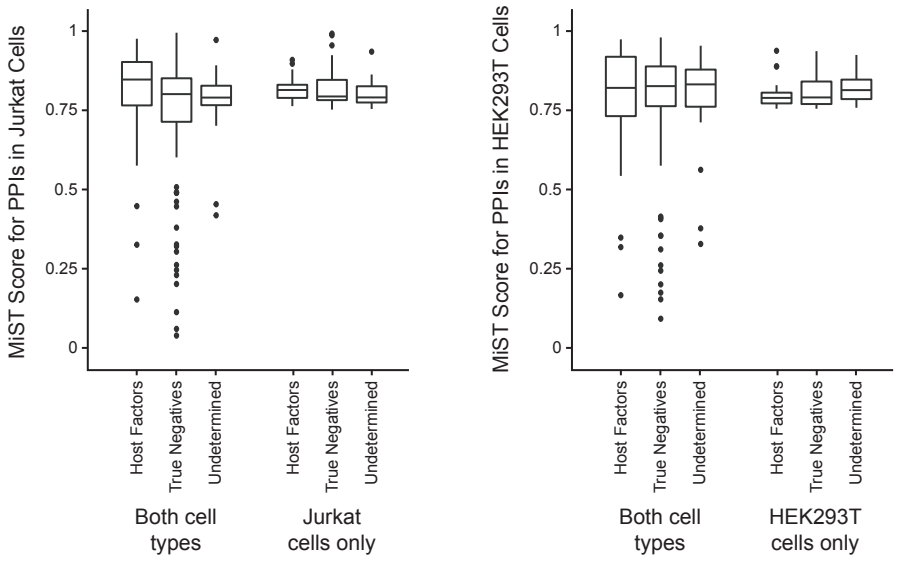
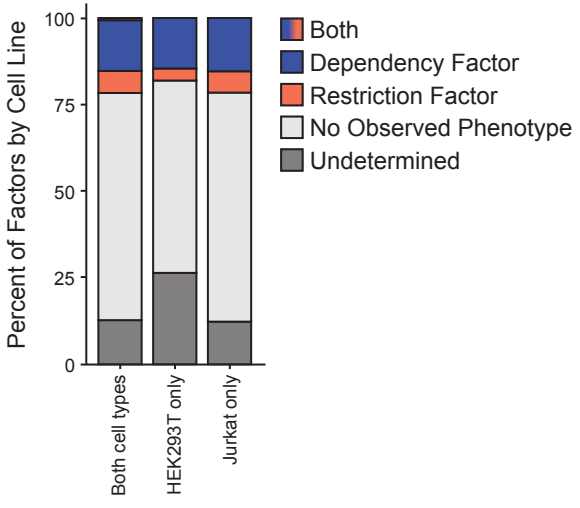


B



Supplementary Figure 5 | Comparison of results to published genome-wide RNAi studies.

a, Number of genes that overlap published genome-wide RNAi screens for HIV host factors, sorted by phenotype in this screen. 'Any' (red) indicates overlap with at least one of the four indicated screens. **b**, Venn diagram indicating the overlap between the candidate dependency factors identified in this screen and the results of published RNAi screens for HIV host factors. Only dependency factors were compared as none of the previously-published screens identified significant restriction factors, and only one reported perturbations that led to increased HIV replication².

A**B**

Supplementary Figure 6 | Analysis of proteomic parameters by genetic phenotype. a, The distribution of reported proteomic probability scores calculated by the MiST algorithm categorized by HIV phenotype and cell type³. Center line, median; box limits, upper and lower quartiles; whiskers, 1.5x interquartile range; black points, outliers. **b,** Cumulative distribution of HIV phenotypes by the cell line in which the protein interaction was identified.

SUPPLEMENTARY REFERENCES

- 1 Finan, C. *et al.* The druggable genome and support for target identification and validation in drug development. *Sci Transl Med* **9**, doi:10.1126/scitranslmed.aag1166 (2017).
- 2 Zhou, H. *et al.* Genome-scale RNAi screen for host factors required for HIV replication. *Cell Host Microbe* **4**, 495-504, doi:10.1016/j.chom.2008.10.004 (2008).
- 3 Jager, S. *et al.* Global landscape of HIV-human protein complexes. *Nature* **481**, 365-370, doi:10.1038/nature10719 (2011).